Enhancement of mechanical performance of epoxy/carbon fiber laminate composites using single-walled carbon nanotubes

Ashrafi, Behnam; Guan, Jingwen; Mirjalili, Vahid; Zhang, Yunfa; Chun, Li; Hubert, Pascal; Simard, Benoit; Kingston, Christopher T.; Bourne, Orson; Johnston, Andrew

Publisher's version / Version de l'éditeur:
https://doi.org/10.1016/j.compscitech.2011.06.015
Composites Science and Technology, 71, 13, pp. 1569-1578, 2011-07-08

Composites Science and Technology 71 (2011) 1569–1578

Contents lists available at ScienceDirect

Composites Science and Technology

journal homepage: www.elsevier.com/locate/compscitech

Enhancement of mechanical performance of epoxy/carbon fiber laminate composites using single-walled carbon nanotubes

Behnam Ashrafi [a,*], Jingwen Guan [b], Vahid Mirjalili [c], Yunfa Zhang [a], Li Chun [a], Pascal Hubert [c], Benoit Simard [b], Christopher T. Kingston [b], Orson Bourne [b], Andrew Johnston [a]

[a] Structures and Materials Performance Laboratory, Institute for Aerospace Research, National Research Council, 1200 Montreal Road, Ottawa, Ontario, Canada K1A 0R6
[b] Molecular and Nanomaterial Architectures Group, Steacie Institute for Molecular Sciences, National Research Council, Ottawa, 100 Sussex Dr., Ontario, Canada K1A 0R6
[c] Department of Mechanical Engineering, McGill University, 817 Sherbrooke Street West, Montreal, QC, Canada H3A 2K6

ARTICLE INFO

Article history:
Received 4 February 2011
Received in revised form 16 June 2011
Accepted 28 June 2011
Available online 8 July 2011

Keywords:
A. Carbon nanotube
A. Carbon fiber
B. Impact behavior
B. Interface
Multiscale composites

ABSTRACT

Carbon nanotubes (CNT) in their various forms have great potential for use in the development of multifunctional multiscale laminated composites due to their unique geometry and properties. Recent advancements in the development of CNT hierarchical composites have mostly focused on multi-walled carbon nanotubes (MWCNT). In this work, single-walled carbon nanotubes (SWCNT) were used to develop nano-modified carbon fiber/epoxy laminates. A functionalization technique based on reduced SWCNT was employed to improve dispersion and epoxy resin-nanotube interaction. A commercial prepregging unit was then used to impregnate unidirectional carbon fiber tape with a modified epoxy system containing 0.1 wt% functionalized SWCNT. Impact and compression-after-impact (CAI) tests, Mode I interlaminar fracture toughness and Mode II interlaminar fracture toughness tests were performed on laminates with and without SWCNT. It was found that incorporation of 0.1 wt% of SWCNT resulted in a 5% reduction of the area of impact damage, a 3.5% increase in CAI strength, a 13% increase in Mode I fracture toughness, and 28% increase in Mode II interlaminar fracture toughness. A comparison between the results of this work and literature results on MWCNT-modified laminated composites suggests that SWCNT, at similar loadings, are more effective in enhancing the mechanical performance of traditional laminated composites.

1. Introduction

Carbon nanotubes (CNT) have shown great promise for use in development of multifunctional multiscale laminated composites. CNT can be incorporated within a fiber reinforced plastic structure through integration with the matrix [1], fiber [2] or both [3]. The main advantage of CNT in such applications is their potential to address several weaknesses of conventional laminated composites including delamination problems, low impact damage resistance, weak fiber–matrix interface, and low transverse mechanical properties. Integration of CNT within the resin matrix mainly addresses resin-dominated properties such as delamination, impact resistance and transverse properties. On the other hand, incorporating CNT into the sizing of conventional fiber reinforcements has the potential to improve fiber/matrix adhesion, mainly via a large increase in the effective surface area of the fiber. Whether they are integrated into the fiber or the matrix resin, CNT-modified composite laminates have usually been fabricated using liquid molding methods such as vacuum-assisted resin transfer molding, or VARTM [1,4,5]. However, a key challenge with using this method is the very large increase in resin viscosity that accompanies CNT introduction. To address this issue and to support commercialization of CNT-modified hierarchical composites, prepregging has also been examined for the integration of modified resins with the reinforcing fibers [6–8].

Epoxies are widely used as the polymer matrix for high-performance laminated composites due to their good mechanical performance, processability, compatibility with most fibers, chemical resistance, wear resistance and cost. However, these materials are relatively brittle, which is detrimental to the interlaminar properties. The addition of soft nano-particles (SNP) has demonstrated great potential to improve the mechanical performance of thermosets and their laminates. While several mechanisms have been proposed to explain such improvements, crack-pinning is frequently cited as one of the key enhancement mechanisms [9]. In recent years, rigid nano-particles such as CNT have shown the potential to act as toughening agents for a range of epoxies due to their high aspect ratios and excellent mechanical properties. CNT toughening mechanisms are mainly based on fiber bridging (fiber pull-out and fracture) and are thus different from those of SNP. It

* Corresponding author. Tel.: +1 613 993 2413; fax: +1 613 998 8609.
E-mail address: behnam.ashrafi@nrc-cnrc.gc.ca (B. Ashrafi).

0266-3538/$ - see front matter Crown Copyright © 2011 Published by Elsevier Ltd. All rights reserved.
doi:10.1016/j.compscitech.2011.06.015

is therefore reasonable to hypothesize that a combination of the two types of nanoparticles could result in synergistic enhancements of fracture toughness.

Of the two main categories of CNT, single-walled CNT (SWCNT) and multi-walled CNT (MWCNT), the latter have been more widely utilized for the development of enhanced hierarchical laminated composites (readers can refer to a recent review paper on the subject by Qian et al. [10]), due to their low cost, commercial availability in large quantities and ease of dispersion. As a result, the potential of SWCNT for use in hierarchical composites is largely unknown. Some studies, however, have shown that SWCNT offer superior performance due to their smaller diameter (or higher surface areas), higher aspect ratios, more efficient load transfer and better mechanical properties due to higher crystallinity [11,12]. On the other hand, SWCNT are known to pose challenges in terms of dispersion, requiring the development of suitable functionalization techniques which address these issues while not damaging the SWNCT molecular structure.

This work focuses on production and characterization of SWCNT-modified (hierarchical) carbon fiber/epoxy laminated composites. An epoxy system already optimized for toughness through incorporation of conventional modifiers was chosen as the baseline material. To develop a SWCNT-modified version of this epoxy, a functionalization scheme based on reduced SWCNT was utilized since it provided both uniform SWCNT dispersion within the epoxy and covalent bonding between the SWCNT and the epoxy matrix. The end-notch fracture toughness (ENF) of different batches of modified epoxy containing 0.1 wt% or 0.2 wt% of SWCNT were compared with the baseline epoxy resin. Based on these results, unidirectional carbon fiber prepreg sheets made of 0.1 wt% functionalized SWCNT-modified epoxy resin were manufactured for further mechanical testing, including impact and compression-after impact tests and fracture toughness tests (both Mode I and Mode II). Non-destructive techniques (ultrasonic C-scan and scanning electron microscopy) were also used to evaluate effects of SWCNT on the performance of the laminated composites.

2. Materials

SWCNT were produced in-house using a double-laser method reported previously [13]. The produced pristine SWCNT were purified using an NRC-developed purification procedure known as WCPP (Wet Chemistry Purification Protocol), mentioned in other recent publications [14,15]. Tube purity after purification is greater than 90% by weight (Fig. 1). An epoxy resin system (Bisphenol A-(epichlorohydrin) provided by Newport), already optimized for toughness using a plasticizer, was used in this work. To functionalize the tubes, SWCNT in the form of dry powder were ground in a small amount of dry Tetrahydrofuran (THF) within an agate mortar, and then the wet paste was transferred into a Schlenk flask. After adding more THF, the mixture was bath-sonicated until a well-dispersed suspension was formed. The suspension was purged with nitrogen and mixed with small pieces of sodium to dry the mixture. After stirring for 20 min, a previously-prepared dark green sodium–naphthalene–THF solution was added to the mixture. The mixture immediately became dark green and was stirred at room temperature for roughly 24 h, then centrifuged at 5000 RPM for 30 min. The liquid phase was discarded and the precipitate was washed twice with dry THF, then again suspended in dry THF for next step. A THF-based solution of the epoxy system (pre-mixed with plasticizers) was heated to 65 °C in a 4 L beaker and sparged with nitrogen for 30 min while being subjected to strong mechanical stirring. Under continuous nitrogen flow and at constant temperature, the reduced SWCNT suspension in THF was quickly poured into the hot resin solution over a 10-minute period. The chemical strategy utilized for the integration of reduced SWCNT and the epoxy system is presented in Fig. 2. After all the SWCNT suspension was added, the mixture was strongly stirred for an additional 2 h, while being maintained at 65 °C, while a strong flow of nitrogen was blown onto the surface. The nitrogen gas was then replaced by compressed air and sparging continued for another 2 h at the same temperature. Finally, the remaining resin mixture was placed in a vacuum oven at 100–120 °C and a pressure of about 1 torr overnight until no solvent smell was detected. Details about the method used to functionalize the SWCNT are provided elsewhere [16].

Two batches of SWCNT-integrated epoxy system with loadings of 0.1 wt% and 0.2 wt% were prepared according to this functionalization scheme. Two other samples of nano-modified epoxy system with similar loadings of SWCNT were also prepared using a surfactant (BYK-67A) in order to reduce air bubble formation. A small amount of surfactant (0.2 wt%) was added to the resin by hand stirring for 5 min. Based on results from characterization of small batches of the SWCNT-modified epoxy system (See Section 4.1), resin using 0.1 wt% reduced SWCNT with the surfactant was chosen for fabrication of SWCNT-modified carbon fiber laminates. After preparing 20 kg of this SWCNT-modified epoxy system, using the methods described above, a prepreg tow processing technique was used to impregnate unidirectional carbon fiber tape (Newport Graphite Unitape G150 NASS) using a commercial-scale solvent-free prepregging technique based on hot melt processing. To reduce impregnation time and minimize potential resin degradation due to extended heating, the compact fiber tows were first expanded transversely before resin was applied to both sides [17]. Prepreg sheets 92 mm wide by 0.155 mm thick were made from both non-modified (baseline) and SWCNT-modified resins using a commercial prepregger machine at 60 °C. In order to compensate

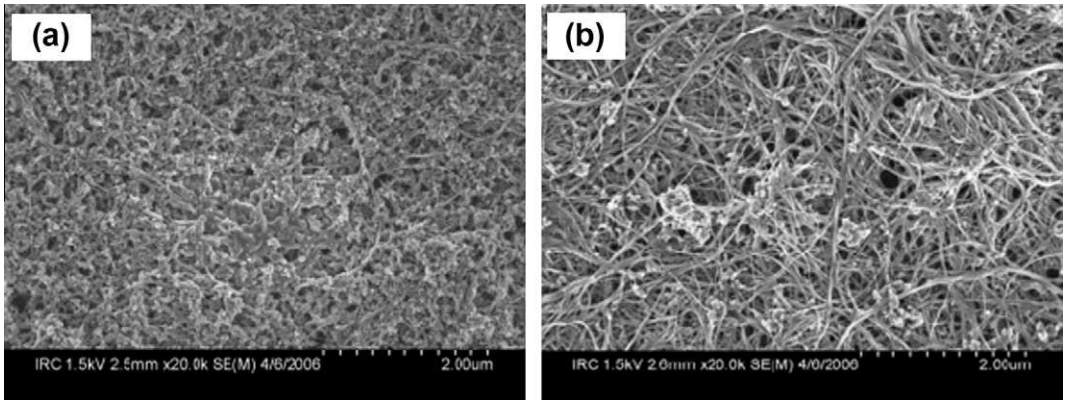

Fig. 1. SEM images of (a) as-produced SWCNT and (b) purified SWCNT.

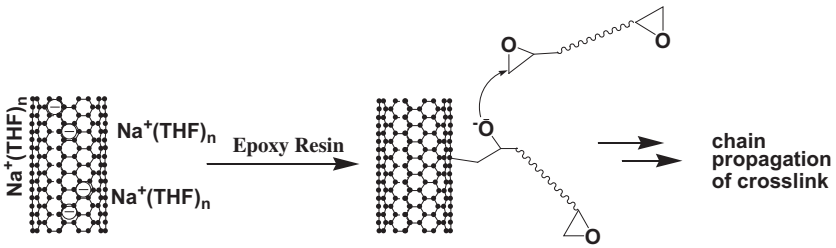

Fig. 2. Functionalization scheme based on negative charging for the integration of SWCNT and epoxy.

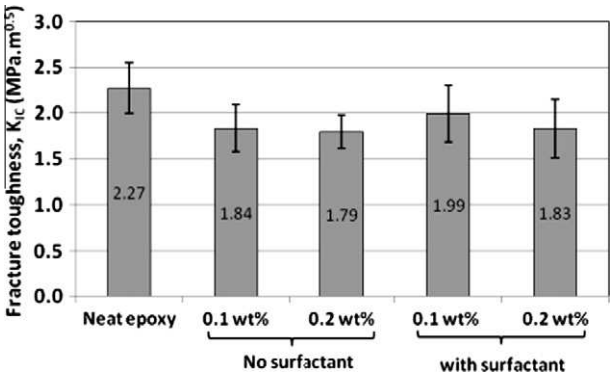

Fig. 3. Effect of SWCNT on resin fracture toughness.

for the viscosity change arising from the addition of SWCNT, prepregging speed was adjusted to obtain comparable impregnation quality for both baseline and SWCNT-modified prepreg. After prepregging, the material was stored in a freezer at −22 °C. Composite panels were manufactured using an autoclave after typical manual hand layup and vacuum bagging of prepreg plies.

3. Methods

3.1. Resin fracture toughness tests

Plane-strain fracture toughness (K_{IC}) was measured on samples of neat resin (no CNT), and four nanocomposite batches made using SWCNT with loadings of 0.1 and 0.2 wt% (with and without surfactant). All neat and SWCNT-modified epoxy resins were cured at 130 °C for 2 h. For each resin batch, six coupons of dimensions $40 \times 9.5 \times 4.75$ mm^3 were cut from cast blocks using a diamond saw. Coupons were lightly sanded with 400-grit sandpaper to smooth rough edges and improve the surface finish. A sharp notch 0.9 mm wide was machined into the specimen using a milling machine with a Dremel rotary disk which generated a flat bottom notch. A sharp natural crack was then generated by sliding a new razor blade across the root notch to create a total crack length (a) of $0.45 < \frac{a}{b} < 0.55$ (b: specimen width), in accordance with ASTM D 5045 [18].

3.2. Mode I and Mode II interlaminar fracture toughness

In order to evaluate effects of SWCNT on the ability of the laminate to resist interply delamination under a normal force perpendicular to the crack plane (Mode I) and a shear force (Mode II), both Mode I and Mode II interlaminar fracture toughness tests were performed on the laminates. Panels with dimensions of $280 \times 165 \times 3.8$ mm^3 were manufactured from each of the two batches of prepreg (i.e. with and without SWCNT). Panels were made of 24 layers of unidirectional prepreg plies with a Teflon film of $280 \times 63.5 \times 0.012$ mm^3 inserted between the 12th and 13th plies along one edge of the layup. Both laminates were cured at 130 °C for 70 min with a temperature ramp rate of 2 °C min for heating and cooling. Double cantilever beam (DCB) specimens for both Mode I and Mode II fracture tests were cut from each panel using a water-cooled diamond table saw in accordance with ASTM D5528 [19]. Mode I tests were performed in displacement control at a loading rate of 0.5 mm/min and unloading rate of 25 mm/min. Load frame crosshead displacement and load were captured in 2 s intervals. Load and displacement were then related to delamination length as measured with a ruler on the specimen edge. For each of the material systems, five specimens were tested to obtain average value of initiation and propagation G_{IC} Mode II fracture tests were performed using the end-notch flexure test (ENF) [20]. Two Mode II interlaminar fracture toughness values, non-precracked (NPC) toughness and precracked (PC) toughness, were calculated for each sample. The NPC toughness was calculated at the initial onset of delamination growth, starting at the edge of the embedded Teflon insert, while the PC toughness was calculated after delamination had already advanced beyond the implanted Teflon insert. Delamination growth was found to be highly unstable in Mode II, so only initiation values for fracture toughness were ultimately obtained. The fracture tests and required compliance calibration were done using a three-point bending fixture with an MTS Insight® Electromechanical Testing System at a displacement rate of 0.5 mm/min in loading, 1.6 mm/min in unloading, and a sampling rate of 30 data/min.

3.3. Impact and post impact tests

Impact damage resistance and compression-after-impact (CAI) strength of composite laminates were determined using the standard test methods described in ASTM D7136 and ASTM D7137 [21,22]. For each of retained material systems (unmodified resin and resin with 0.1 wt% functionalized SWCNT), a 5 mm thick laminate panel with a stacking sequence of $[45/0/-45/90]_{4S}$, which is a quasi-isotropic, mid-plane symmetric, was manufactured using an autoclave. Both laminates were cured at 130 °C for 70 min with a temperature ramp rate of 2 °C min for heating and cooling. From each panel, six coupons with dimensions $152 \times 102 \times 5.0$ mm^3 in thickness were cut using a diamond saw. The 0° ply was aligned with the long dimension of the panel according to the ASTM standard. All specimens were impacted using a Dynatup® Model 8200 drop weight impact machine. Specimens were placed on a support fixture over a 76.2 mm × 127.0 mm rectangular cut-out in the impactor base and held in place by four rubber-tipped clamps to exert clamping pressure. A hardened steel 15.9 mm diameter hemispherical striker (impact tip) with an overall impactor weight of 6.3 kg was used. All impact tests and subsequent compression-after-impact (CAI) strength tests were conducted at laboratory ambient conditions. Impact damage was assessed via ultrasonic C-scan using a TecScan seven axis automated ultrasonic system including an Utex pulser/receiver, Tecscan data acquisition software and a 2.25 MHz, 12.7 mm diameter immersion probe [23].

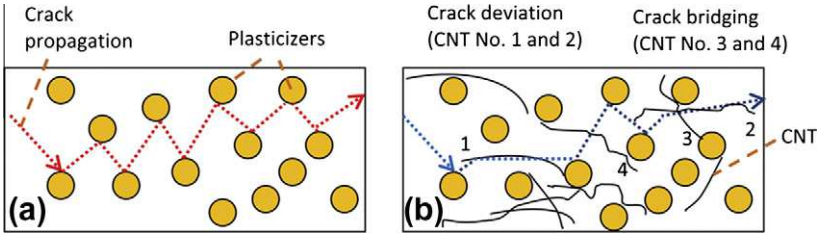

Fig. 4. Schematic of the effects of SWCNT and plasticizers on fracture toughness. (a) Crack-pinning mechanism arising from SNP inclusion within the resin. (b) The conflicting influence of CNT on the crack propagation: both bridging cracks (for CNT numbered as 3 and 4) and diverting crack around SNP due to a weaker CNT-epoxy interface (for CNT numbered as 1 and 2).

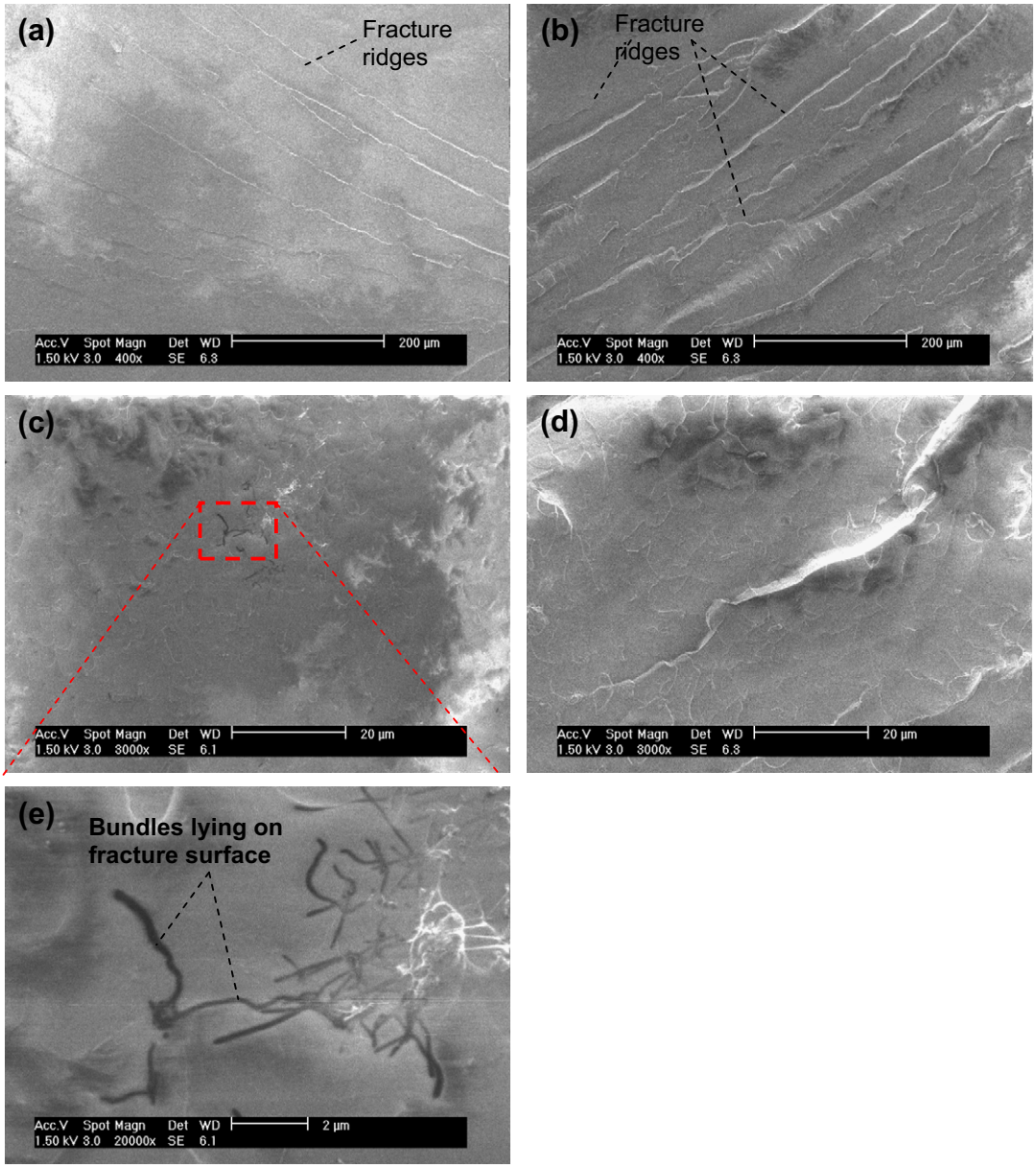

Fig. 5. SEM images taken from fractured surfaces of a SWCNT-modified epoxy resin specimen (a, c and e) and a neat epoxy specimen (b and f); a comparison of the fractured surfaces at a low magnification (a and b) and a high magnification (c and d) suggests a rougher surface for neat fractured surface; The existence of individual bundles of SWCNT lying on the fracture surface of the nanocomposite sample (e).

Measurements of damage extent were conducted based on digital C-Scan images using Matlab software by estimating the maximum extend of delamination damage. To evaluate the CAI strength of coupons, compressive load was applied at a rate of 1.27 mm/min under cross-head displacement control using a 450 kN load capacity MTS 880 hydraulic load frame according to ASTM D7136. The

CAI test fixture provides supports to the vertical edges of the specimen to prevent buckling, and the top and bottom edges are clamped to suppress edge delamination.

4. Results and discussion

4.1. End-notch fracture toughness tests

Fig. 3 shows the measured fracture toughness for five different resin batches: neat epoxy; 0.1 wt% and 0.2 wt% SWCNT (without surfactant); 0.1 wt% and 0.2 wt% SWCNT (with surfactant). All thirty test results (six per each batch) were deemed valid since the loading relationship was linear in each case, with an abrupt drop to zero at the instant of crack growth initiation. Fracture surfaces were examined using microscopy to identify any voids on the fracture surface. Only one out of 30 tested specimens was found to contain voids on the fracture surface (it was eliminated from the data). The average and standard deviation of the calculated plane-strain fracture toughnesses for each batch are shown in Fig. 3. For all four batches of nanocomposites, the addition of SWCNT resulted in a reduction in fracture toughness (12–20%) as compared to the neat epoxy system. One possible explanation for this reduction is illustrated in Fig. 4. As discussed previously, the addition of plasticizers causes an increase of fracture toughness versus unmodified epoxy through a crack pinning mechanism (Fig. 4a). Optimization of the plasticizer content therefore results in maximizing crack-pinning effectiveness. Although the addition of SWCNT can also potentially enhance the fracture toughness of an epoxy system via various mechanisms such as fiber bridging, they can also reduce the effectiveness of the SNP additives by deviating cracks away from these plasticizers through the weaker resin-SWCNT interface (see Fig. 4b). Hence, although SWCNT can substantially enhance resin toughness in some resins, the net result of their introduction can be a toughness reduction in others (as in this work).

As shown in Fig. 3, increasing SWCNT content from 0.1 wt% to 0.2 wt% results in a further reduction of fracture toughness for both with and without surfactant cases (from 12% to 19% for cases with surfactant and from 19% to 21% for cases without surfactant). This reduction may be attributed to the increasingly negative impact of SWCNT crack path deviation from the SNP. However, other possibilities may explain the observation such as increased resin viscosity during processing [24], modifications to the cure rate and molecular network formation [25]. In any case, the data suggest

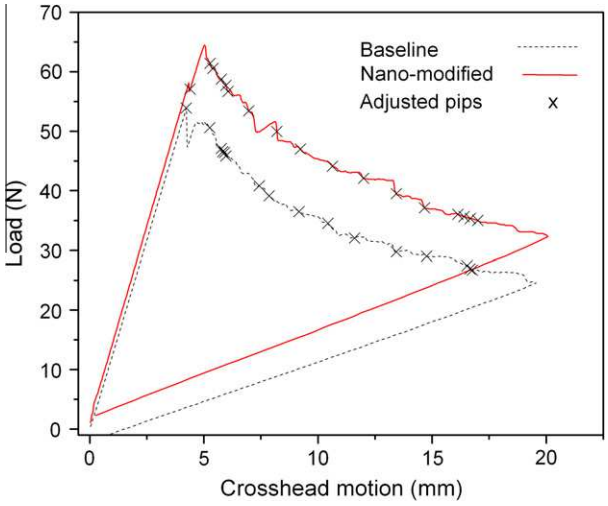

Fig. 6. Load–displacement curves of neat and SWNT modified DCB samples.

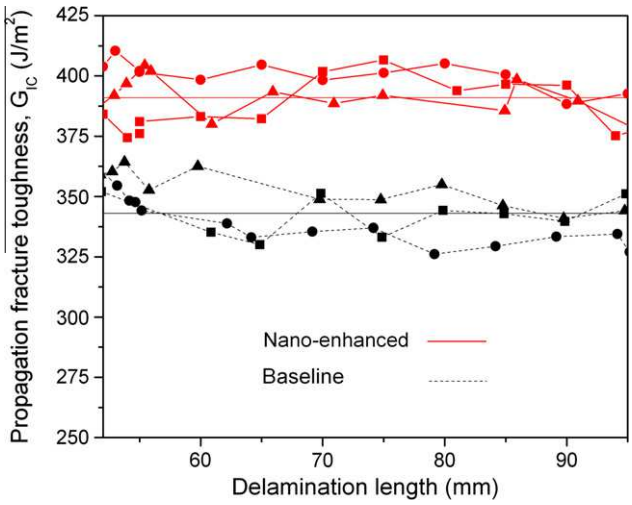

Fig. 7. Fracture resistance curve values comparing neat versus SWNT modified DCB samples.

Table 1
Comparison summary of mechanical testing of neat and nano-modified laminates.

Properties	Unmodified laminate	SWCNT-modified laminate	Percentage increase/decrease (%)
G_{Ic} Initiation	314 ± 18 J/m^2	323 ± 41 J/m^2	+3.0
G_{Ic} Propagation	343 ± 7 J/m^2	387 ± 6 J/m^2	13.0
G_{IIc} Non precracked	1.79 ± 0.24 KJ/m^2	2.01 ± 0.13 KJ/m^2	12.4
G_{IIc} Precracked	1.10 ± 0.13 KJ/m^2	1.41 ± 0.08 KJ/m^2	27.4
Area of impacted zone (mm^2)	57.8 ± 4.8	54.8 ± 4.0	−5.2
Residual compression strength (σ_c)	228 ± 11 MPa	235 ± 3 MPa	+3.5

that the addition of surfactant reduces the negative effect of SWCNT on resin toughness for both CNT loading levels, perhaps by reducing air bubbles.

Fig. 5 shows SEM images taken from bulk samples of epoxy nanocomposite with 0.1 wt% SWCNT (with surfactant) and neat epoxy. At magnifications of both 400× and 3000×, the fracture surface of the neat epoxy (Fig. 5b and d) seems to be rougher (more ridges) than that of the nanocomposite (Fig. 5a and c), suggesting that more energy was required for crack propagation in the neat epoxy specimens. This is in agreement with the results presented in Fig. 3 and the hypothesis presented in Fig. 4. Fig. 5e shows the higher magnification image of the nanocomposite fracture surface, demonstrating the existence of individual SWCNT bundles lying on the fracture surface. This is a possible reason for the smoother nanocomposite fracture surface as compared with the neat epoxy, in agreement with the assumptions for crack deviation presented in Fig. 4.

4.2. Modes I and II interlaminar fracture toughness

Due to the marginally better end-notch fracture toughness results obtained, resin formulations with 0.1 wt% SWCNT (with surfactant) were chosen for fabrication of composite laminates, along with the baseline resin containing no CNT.

Load–displacement curves comparing neat and SWCNT-modified Mode I DCB specimens show a linear load–displacement

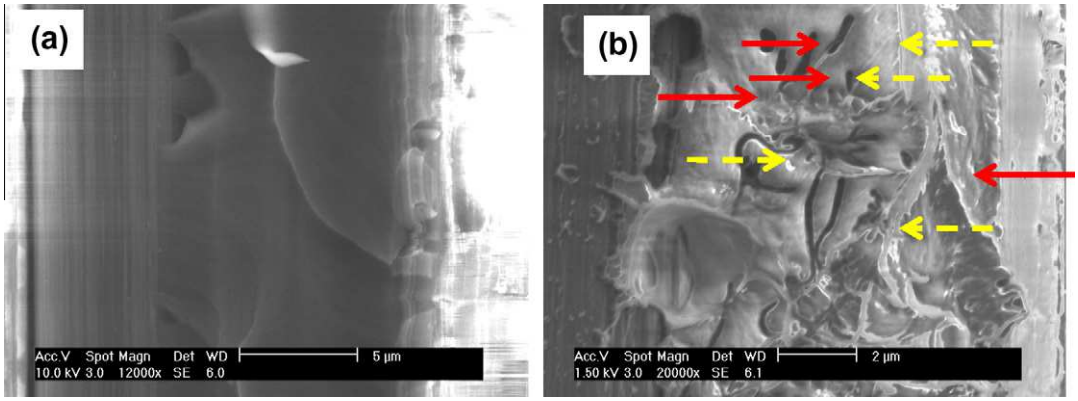

Fig. 8. SEM images of DCB coupons failed under Mode I loading for (a) baseline laminate and (b) SWCNT-modified laminate. Evidence of two types of crack bridging can be seen for larger bundles of SWCNT: CNT pull-out for bundles more perpendicular to the fracture surface, shown by red arrows, and CNT peeling-out for bundles more parallel to the fracture surface, shown by dotted yellow arrows.

relationship up to the point of crack initiation (Fig. 6). However, SWCNT-modified samples sustained a higher crack-initiation load. The load–displacement data were used to generate fracture resistance curves as shown in Fig. 7. As can be seen, the fracture toughness values were nearly independent of crack length for all six specimens shown in Fig. 7. This compares to other published results based on MWCNT [26,27] in which the fracture toughness values vary considerably as crack length increases. It seems reasonable that this may be attributable to a more uniform dispersion of SWCNT within epoxy due to a lower loading of SWCNT and the effective functionalization to maintain the dispersion. G_{Ic} initiation and propagation measurements for all specimens were averaged and reported in Table 1. As shown in the table, Mode I interlaminar initiation toughness values were found to be lower than propagation values. This is believed to be caused by the fact that the first incremental delamination starts from the end of the Teflon insert (crack initiator) and it is only after the crack begins to propagate that toughening mechanisms such as fiber bridging begin to act, increasing the energy required to grow the crack further [28–30]. Fig. 8[1] shows an SEM image of a fractured DCB coupon failed under Mode I loading. This figure shows evidence of bridging by larger bundles of SWCNT, contributing to the observed increase of fracture toughness failure via two different mechanisms: pull-out of SWCNT bundles that were near-perpendicular to the fracture surface (shown by red arrows in the figure), and a peeling or combined peeling/pull-out mechanism for nanotubes more parallel to the fracture surface, shown by dotted yellow arrows.

It is interesting to note that the initiation G_{Ic} for the SWCNT-modified laminates was 3% higher than for the neat DCB samples while the average propagation value increased by 13%. Since the SWCNT toughening mechanisms postulated above are expected to be more "active" during propagation, this supports the idea that these are indeed the source of the increased toughnesses observed. A similar increase of 13% in Mode I fracture toughness was reported by Romhany and Szebenyi [27] for a MWCNT loading of 0.3 wt%, suggesting that SWCNT may be more effective than MWCNT for a given loading. In another work, Karapappas et al. [31] demonstrated that 1 wt% loading of MWCNT can result in a 60% improvement in Mode I fracture toughness; however, for small loading of 0.1 wt% (similar to this work) slight reductions in both Mode I and Mode II fracture toughness values were reported.

Fig. 9 shows an example of load–displacement measurements during Mode II fracture toughness tests for both baseline and nano-composite samples. The percentage change in the Mode II interlaminar fracture toughness values after addition of SWCNT is listed in Table 1. Increases of 12% and 27% were measured for pre-cracked (PC) and non-precracked (NPC) coupons, respectively, upon addition of SWCNT. Fig. 10 shows SEM images of the fracture surfaces of a baseline and a nano-modified specimen. Two dominant toughening mechanisms involved with Mode II fracture tests are micro-cracks and hackles, which are both related to micro-scale matrix failure modes [22–37]. A comparison between the two SEM images shows that the hackles are larger for the nano-composites. Unlike the Mode I DCB specimens, which exhibit continuous crack growth along the fiber/matrix interface, Mode II ENF specimens show discontinuous crack growth by micro-crack coalescence, leading to the development of hackles at the fracture surface. In Mode II loading, fiber bridging is a less important toughening mechanism than in Mode I failure [30,38]. It is postulated that in Mode II nanotube bundles act as rigid fillers which arrest the crack, preventing or delaying the expansion of micro-cracking within the matrix-rich interface area. That would explain the larger hackles present at the fracture surface of the CNT modified composite laminates as compared to that of the base composite laminates. Fig. 10c and d shows higher magnification SEM images of fractured specimens. Some level of fiber bridging by larger CNT bundles can be seen in the nano-modified laminates.

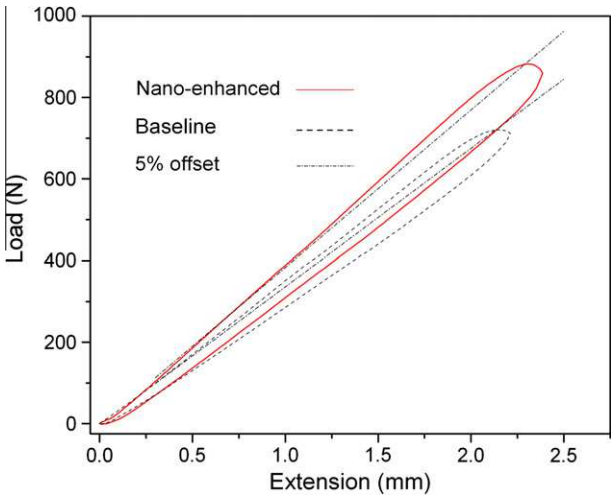

Fig. 9. A representative graph showing the Mode II fracture tests for the nano-enhanced and baseline samples.

[1] For interpretation of color in Figs. 8 and 13, the reader is referred to the web version of this article.

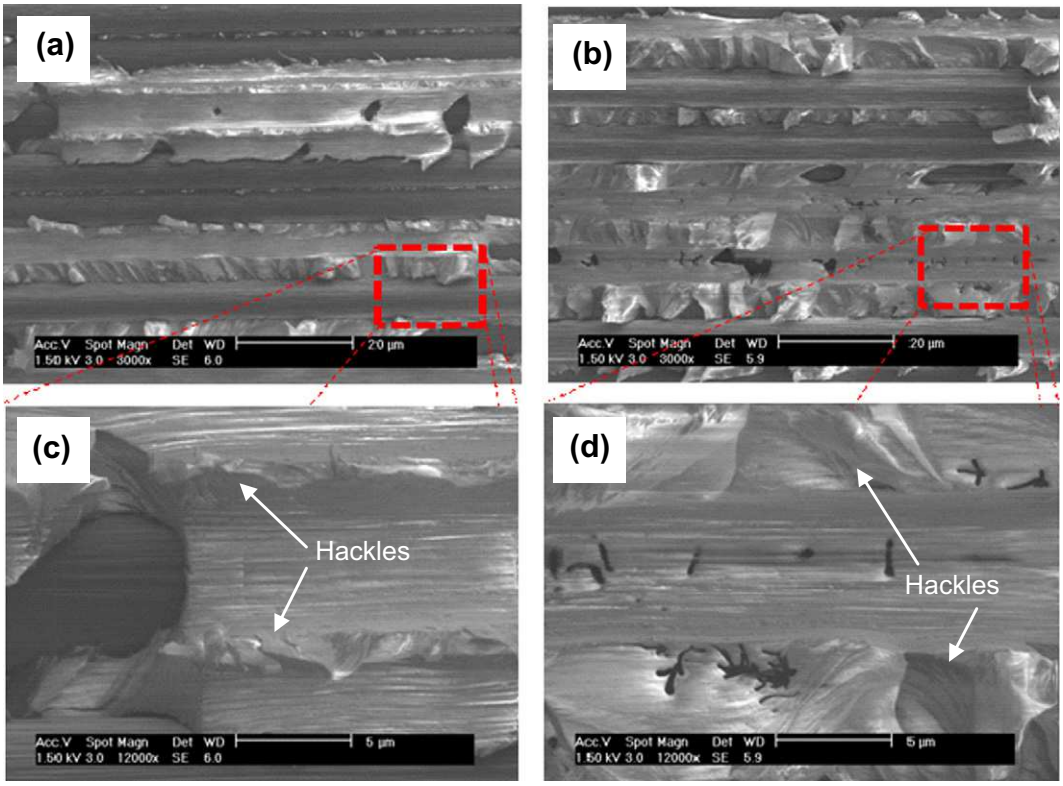

Fig. 10. SEM of fractured Mode II DCB coupons at different magnifications for (a and c) baseline laminate and (b and d) SWCNT-modified laminate. The existence of larger hackles can be seen for SWCNT-modified laminate.

As summarized in Table 1, the addition of a small quantity of SWCNT resulted in considerable improvements in both Mode I and Mode II fracture toughness values. It has been previously shown that an increase of interlaminar layer thickness can result in an increase of interlaminar fracture toughness [39,40]. Due to the increase in resin viscosity that accompanies the addition of CNT, is has been suggested (e.g. by Quan et al. [10]) that this may be the source of previously observed toughness increases rather than any direct effects of the CNT themselves. In order to rule out this possibility for the current case, optical microscopy of cross-sections of both baseline and SWCNT-modified laminates was conducted (an example shown in Fig. 11). This study revealed no difference in the overall thickness of the resin-rich layer between plies, nor were any significant differences found in the total thicknesses of the two different types of laminates (i.e. with and without SWCNT).

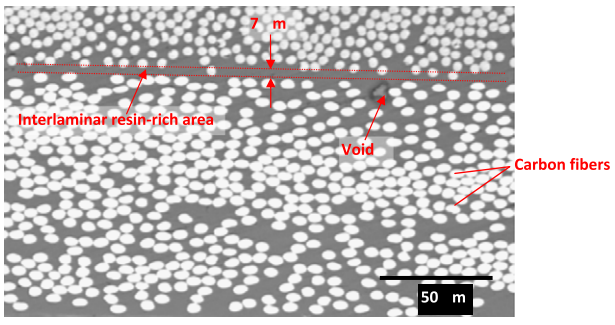

Fig. 11. A microscopic image of the interlaminar region between two adjacent layers of the nano-modified laminates. A small void of a few micrometers is also visible near the interface.

The measured improvements in ModeS I and II interlaminar fracture toughness with the addition of SWCNT are contrasted with the 12% *reduction* observed in resin fracture toughness for the same case. Two sources for this contradiction are hypothesized. First, during resin end-notch fracture toughness tests, the crack front has the freedom to propagate in any directions (locally). As a result, cracks can progress along the length of a SWCNT (or bundle of SWCNT), which is likely the lowest energy mode for crack growth. For the case of laminate Mode I and Mode II interlaminar fracture toughness tests, however, crack growth is limited to the 7 μm-thick interlaminar layer (Fig. 11). As a result, SWCNT that pass through this region can effectively bridge the crack front, as shown in Fig. 8.

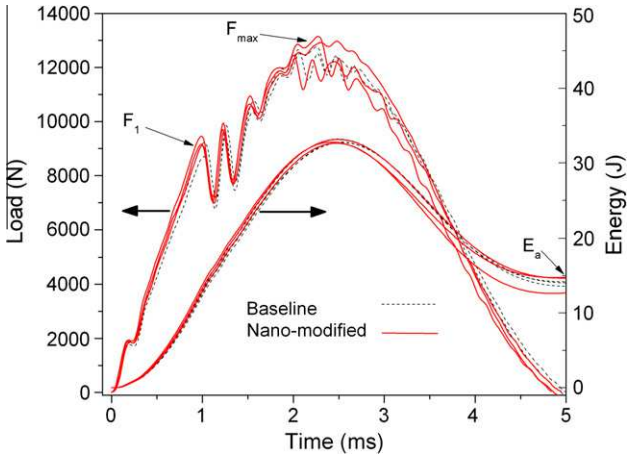

Fig. 12. Load and absorbed energy versus time for three baseline and three nano-modified coupons.

Table 2
Impact response parameters and compression-after-impact strength of baseline and nano-modified laminates.

	F_1 (KN)	F_{max} (KN)	E_J (J)	E_a (J)	Damage area (cm^2)	Strength (MPa)
Baseline specimens						
Coupon 1	8.94	12.3	32.4	13.6	58.9	236
Coupon 2	9.23	12.7	32.9	14.2	54.6	240
Coupon 3	8.71	12.8	32.5	14.0	51.6	224
Coupon 4	9.27	12.8	32.5	14.8	59.2	219
Coupon 5	9.50	12.2	32.4	14.2	65.5	212
Coupon 6	9.06	12.9	32.4	12.6	56.9	238
	9.12 ± 0.28	12.6 ± 0.3	32.5 ± 0.2	13.9 ± 0.7	57.8 ± 4.8	228 ± 11
SWCNT-modified specimens						
Coupon 1	9.16	12.5	32.8	14.7	57.4	–
Coupon 2	9.46	13.2	32.5	14.7	53.8	240
Coupon 3	9.12	13.0	32.3	12.6	61.5	232
Coupon 4	9.21	12.7	32.2	13.1	53.1	234
Coupon 5	9.45	12.6	32.5	14.5	52.1	237
Coupon 6	9.17	12.8	32.7	13.6	50.8	237
	9.26 ± 0.15	12.8 ± 0.3	32.5 ± 0.2	13.9 ± 0.9	54.8 ± 4.0	236 ± 3
Difference	+1.57%	+1.33%	+0.08%	+0.36%	−5.2%	+3.5%

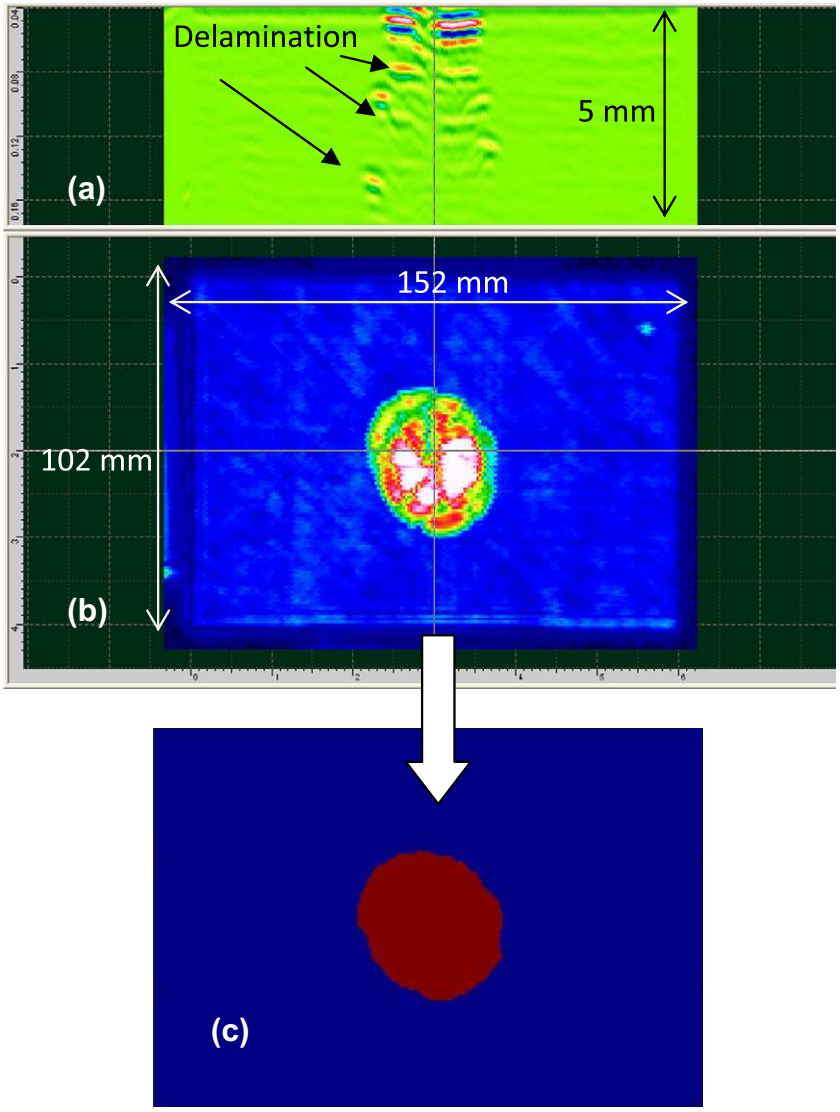

Fig. 13. A representative C-scan image of an impacted panel; (a) B-scan through the thickness; (b) internal damage extent; and (c) calculation of delamination area using a MATLAB code.

A second factor may relate to the fact that while resin end-notch fracture toughness tests were performed on specimens cut from bulk resin, in which SWCNT dispersion is more-or-less random, the process of prepreg manufacturing likely results in

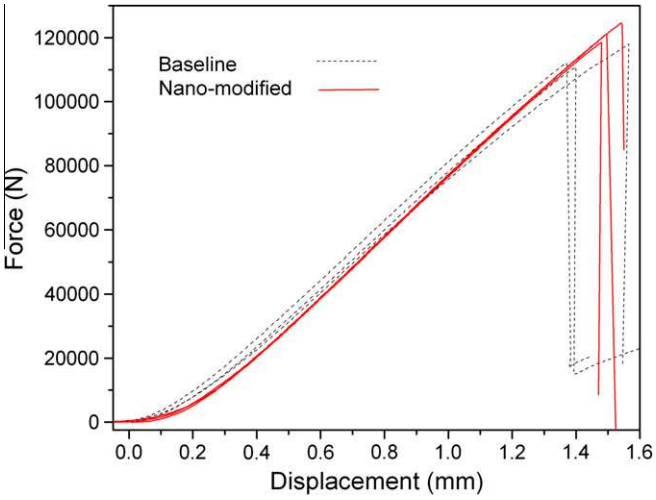

Fig. 14. Compression-after-impact test results for three representative laminates.

changing both the orientation and dispersion of SWCNT. It is likely that thickness-through impregnation of carbon fiber tapes results in a partial alignment of SWCNT, perpendicular to the crack growth direction. In this scenario, SWCNT are to be more effective to bridge the crack and increase the fracture toughness as compared to the randomly-oriented SWCNT in bulk specimens as shown in Fig. 4. Factors other than those mentioned above, can also explain this discrepancy between bulk samples and their composites. As an example, it has been previously shown that a slight reduction in epoxy molecular network density can cause an increase in resin fracture toughness [41]. It is possible that the presence of both SWCNT and carbon fibers in the nano-modified laminate can result in a further reduction of epoxy network density as compared to the baseline epoxy/carbon fiber laminate, resulting in the enhancement of the fracture toughness of the nano-modified laminate.

4.3. Impact resistance and CAI strength

Fig. 12 plots the impact force and the absorbed energy (calculated through the numerical load–time curve integration) versus time for baseline and nano-modified specimens. Only three representative curves for each laminate (out of six specimens tested) are shown for clarity. These graphs show that the tests were very repeatable. As can be seen, an abrupt change in load is evident at about 9 kN, followed by a series of notable load reversals which are most likely caused by progressive failures in individual plies and accompanying load redistributions. The load at which the first evidence of failure is observed is designated as F_1. The maximum load (F_{max}) level is about 13 kN for both types of laminates. As shown in Fig. 12, about 5 ms after the start of impact, the impact force drops to near zero, implying that the impactor is no longer in contact with the specimen and the impact process is complete. The absorbed energy at this instant is thus an indication of the total energy transferred to the specimen. This value is designated as the absorbed energy, E_a, as shown in Fig. 12. The measured loads F_1 and F_{max} (as shown in Fig. 12), the impact energy E_i, and the absorbed energy E_a (also shown in Fig. 12) of all 12 specimens from the two material systems are summarized in Table 2.

The difference in the average values of F_1 and F_{max} for the baseline and nano-modified laminates are 1.6% and 1.3%, respectively, while the difference in the absorbed energy E_a is less than 0.5%. Hence, it is clear that the difference in impact damage response of the two composite systems is, at best, very small. Fig. 13 shows a typical ultrasonic C-scan image of an impacted laminate (showing a baseline specimen). Fig. 13a shows a B-scan image taken a through-thickness "slice" of specimen passing through the centre of the damage area. The delaminated areas, indicated with arrows in the figure, can be seen to increase in size moving from the impact location (top surface) toward the bottom surface of the laminate. Fig. 13b, with the blue background, shows a top view of the internal damage extent. This C-scan image shows all damage throughout the specimen from the top surface to the bottom surface. Hence, this image shows the maximum extent of damage throughout the laminate thickness. Fig. 13c shows a modified version of the C-scan image from Fig. 13b, which was used to calculate the "damage area" of each coupon. After comparing the calculated damage areas of each coupon, it was found out that nano-modified panels have a damage area that is smaller than the baseline panels by an average of 5.2% (Table 2). Given the very similar levels of energy absorption for both types of panels, it is believed that the reduction in damage area can directly be attributed to the contribution of SWCNT to dissipating energy. A similar effect was also observed by Kostopoulos et al. [42] who found that the incorporation of 0.5 wt% MWCNT resulted in a 3% reduction of damage area versus baseline panels. The evidence of greater effectiveness of SWCNT as compared to the MWCNT used in [42] may attributable to their higher aspect ratios (>1000 versus 30–50) and their better mechanical properties. Yokozeki et al. [43] found a similar reduction of 7% in damage area for 10 wt% loading of cup-stacked CNT. Again, the greater effectiveness of SWCNT in this case may be attributable to their much better mechanical properties.

The CAI strength was also obtained for each impacted specimen. Fig. 14 plots compression load versus crosshead displacement for three representative impacted panels from each batch (baseline and nano-modified). The measured CAI strength of all 12 specimens from the two material systems is summarized in Table 2. A 3.5% increase in the compression strength was measured for the nano-enhanced laminates as compared to the baseline panels. However, this result must be used with caution since the results for the baseline specimens have a variance greater than this difference. Comparing these results with others found in the literature, Kostopoulos et al. [42] reported a 12–15% increase in CAI strength for nano-enhanced laminates containing 0.5 wt% MWCNT. Yokozeki et al. [43] measured 0% and 7% in improvements in CAI strength for laminates with 5 wt% and 10 wt% of cup-stacked CNT, respectively.

5. Conclusions

Due to their unique characteristics, CNT have recently attracted significant attention for their potential to be used in development of multifunctional multiscale laminated composites. The primary focus to date has been on MWCNT. In this work, SWCNT were utilized for the development of nano-modified hierarchical carbon fiber/epoxy laminates fabricated using a commercial prepregging technique. Direct integration of CNT within the laminate matrix through prepregging has advantages over methods based on local modification of fibers or interlaminar regions. First, integration can be readily performed on a large scale by minimizing necessary changes in conventional prepreg production methods. Secondly, concerns such as thicknesses increases of interlaminar layers or inhomogeneous laminate reinforcement can be avoided.

In this work, incorporation of 0.1 wt% of SWCNT resulted in a 5% reduction in impact damage area, a 3.5% increase in compression-after-impact strength, 13% increase in Mode I fracture toughness, and 28% increase in Mode II interlaminar fracture toughness. As shown by SEM, SWCNT contribute to increased fracture toughness by crack bridging (pull-out and peeling) in Mode I and the formation of larger hackles in Mode II. A comparison between the results

of this work and literature results on MWCNT-modified laminated composites suggests that SWCNT are more effective in enhancing the mechanical performance of traditional laminated composites. This can be attributed to such factors as their higher aspect ratios, lower levels of impurities, better mechanical properties, and more effective SWCNT-resin interaction through use of an efficient functionalization scheme. However, the optimization of functionalization schemes is necessary to guarantee that higher loadings of nanotubes can be incorporated to the structures to the levels currently achieved by MWCNT (>1 wt%).

Acknowledgments

We are grateful to Mr. Marc Genest for ultrasonic testing and evaluation and Mr. David Chow for SEM imaging.

References

[1] Gojny FH, Wichmann MHG, Fiedler B, Bauhofer W, Schulte K. Influence of nano-modification on the mechanical and electrical properties of conventional fiber-reinforced composites. Compos Part A-Appl S 2005;36:1525–35.
[2] Garcia EJ, Wardle BL, Hart AJ, Yamamoto N. Fabrication and multifunctional properties of a hybrid laminate with aligned carbon nanotubes grown in Situ. Compos Sci Technol 2008;68:2034–41.
[3] Warrier A, Godara A, Rochez O, Mezzo L, Luizi F, Gorbatikh L, et al. The effect of adding carbon nanotubes to glass/epoxy composites in the fiber sizing and/or the matrix. Compos Part A-Appl S 2010;41:532–8.
[4] Fan ZH, Hsiao KT, Advani SG. Experimental investigation of dispersion during flow of multi-walled carbon nanotube/polymer suspension in fibrous porous media. Carbon 2004;42:871–6.
[5] Wichmann MHG, Sumfleth J, Gojny FH, Quaresimin M, Fiedler B, Schulte K. Glass-fiber-reinforced composites with enhanced mechanical and electrical properties – benefits and limitations of a nanoparticle modified matrix. Eng Fract Mech 2006;73:2346–59.
[6] Chen W, Shen H, Auad ML, Huang C, Nutt S. Basalt fiber–epoxy laminates with functionalized multi-walled carbon nanotubes. Compos Part A-Appl S 2009;40:1082–9.
[7] Godara A, Mezzo L, Luizi F, Warrier A, Lomov SV, van Vuure AW, et al. Influence of carbon nanotube reinforcement on the processing and the mechanical behaviour of carbon fiber/epoxy composites. Carbon 2009;47(12):2914–23.
[8] Yokozeki T, Iwahori Y, Ishiwata S, Enomoto K. Mechanical properties of CFRP laminates manufactured from unidirectional prepregs using CSCNT-dispersed epoxy. Carbon 2007;38(10):2121–30.
[9] Ruiz-Perez L, Ryston GJ, Fairclough JPA, Ryan AJ, Toughening by nanostructure. Polymer 2008;49:4475–88.
[10] Qian H, Greenhalgh ES, Shaffer MSP, Bismarck A. Carbon nanotube-based hierarchical composites: a review. J Mater Chem 2010;20:4751–62.
[11] Ma P, Siddiqui NA, Marom G, Kim J. Dispersion and functionalization of carbon nanotubes for polymer-based nanocomposites: A review. Compos Part A-Appl S 2010;41:1345–67.
[12] Cui S, Kinloch IA, Young RJ, Noe L, Monthioux M. The effect of stress transfer within double-walled carbon nanotubes upon their ability to reinforce composites. Adv Mater 2009;21:1–5.
[13] Kingston CT, Jakubek ZJ, Denommee S, Simard B. Efficient laser synthesis of single-walled carbon nanotubes through laser heating of the condensing vaporization plume. Carbon 2004;42:1657–64.
[14] Jakubinek MB, Johnson MB, White MA, Guan JW, Simard B. Novel method to produce single-walled carbon nantoube films and their thermal and electrical properties. J Nanosci Nanotechnol 2010;10:8151–7.
[15] Najafi E, Wang J, Hitchcock AP, Guan JW, Denommee S, Simard B. Characterization of single-walled carbon nanotubes by scanning transmission x-ray spectromicroscopy: purification, order and dodecyl functionalization. J Am Chem Soc 2010;132(26):9020–9.
[16] Guan JW, Martinez-Rubi Y, Denommee S, Ruth D, Kingston CT, Daroszewska M, et al. About the solubility of reduced SWCNT in DMSO. Nanotechnology 2009;20:245701.
[17] Angell RG, Michno MJ, Konrad JM, Hobbs KE. Hot melt prepregg tow process. US patent 4804509, February 14; 1989.
[18] ASTM D 5045. Standard test methods for plane-strain fracture toughness and strain energy release rate of plastic materials. West Conshohocken, PA, USA: ASTM International; 2007.
[19] ASTM D 5528. Standard test method for mode I interlaminar fracture toughness of unidirectional fiber-reinforced polymer matrix composites. West Conshohocken, PA, USA: ASTM International; 2001.
[20] Davidson BD, Sun X. Geometry and data reduction recommendations for a standardized end notched flexure test for unidirectional composites. J ASTM International 2006;3(9):1–19.
[21] ASTM D 7136. Standard test method for measuring the damage resistance of a fiber-reinforced polymer matrix composite to a drop-weight impact event. West Conshohocken, PA, USA: ASTM International; 2005.
[22] ASTM D 7137. Standard test method for compressive residual strength properties of damaged polymer matrix composite plates. West Conshohocken, PA, USA: ASTM International; 2005.
[23] Composite Materials Handbook (MIL-HDBK-17-1F). Polymer matrix composites, guidance for characterization of structural materials. Structural element characterization, vol. 1; 2002. [chapter 7].
[24] Hubert P, Ashrafi B, Adhikari K, Meredith J, Vengallatore S, Guan J, et al. Carbon nanotube composite microactuators: design and characterization. Compos Sci Technol 2009;69:2274–80.
[25] Yang K, Gu M, Jin Y, Mu G, Pan X. Influence of surface treated multi-walled carbon nanotubes on cure behavior of epoxy nanocomposites. Compos Part A-Appl S 2008;39:1670–8.
[26] Garcia EJ, Wardle BL, Hart JA. Joining prepreg composite interfaces with aligned carbon nanotubes. Compos Part A-Appl S 2008;39(6):1065–70.
[27] Romhany G, Szebenyi G. Interlaminar crack propagation in MWCNT/fiber reinforced hybrid composites. Express Polym Lett 2009;3(3):145–51.
[28] Karger-Kocsis J. Stick-slip type crack growth during instrumented high-speed impact of Hdpe and Hdpe/Selr discontinuous laminar microlayer composites. J Macromol Sci B 2001;40(3):343–53.
[29] Webb TW, Aifantis EC. Crack growth resistance curves and stick-slip fracture instabilities. Mech Res Commun 1997;24(2):123–30.
[30] Seyhan TA, Tanoglu M, Schulte K. Mode I and mode II fracture toughness of E-glass non-crimp fabric/carbon nanotube (CNT) modified polymer based composites. Eng Fract Mech 2008;75(18):5151–62.
[31] Karapappas P, Vavouliotis A, Tsotra P, Kostopoulos V, Paipetis A. Enhanced fracture properties of carbon reinforced composites by the addition of multi-wall carbon nanotubes. J Compos Mater 2009;43(9):977–85.
[32] Russell AJ. Micromechanisms of Interlaminar Fracture and Fatigue. Polym Composite 1987;8(5):342–51.
[33] Sue HJ, Jones RE, Garcia-Meitin EI. Fracture behaviour of model toughened composites under mode I and mode II delaminations. J Mater Sci 1993;28(23):6381–91.
[34] Wetzel B, Rosso P, Haupert F, Friedrich K. Epoxy nanocomposites – fracture and toughening mechanisms. Eng Fract Mech 2006;73(16):2375–98.
[35] Kim HS, Ma P. Mode II fracture mechanisms of PBT-modified brittle epoxies. J Appl Polym Sci 1998;69(2):405–15.
[36] Lee JJ, Lim JO, Huh JS. Mode II interlaminar fracture behavior of barbon bead-filled epoxy/glass fiber hybrid composite. Polym Composite 2000;21(2):343–52.
[37] Lee S. Mode II delamination failure mechanisms of polymer matrix composites. J Mater Sci 1997;32(5):1287–95.
[38] Cowley KD, Beaumont PWR. The interlaminar and intralaminar fracture toughness of carbon-fiber/polymer composites: the effect of temperature. Compos Sci Technol 1997;57(11):1433–44.
[39] Singh S, Partridge IK. Mixed-mode fracture in an interleaved carbon-fiber/epoxy composite. Compos Sci Technol 1995;55(4):319–27.
[40] Liu L, Zhang B, Wu Z, Wang D. Effects of cure pressure induced voids on the mechanical strength of carbon/epoxy laminates. Mater Sci Technol 2005;21(1):87–91.
[41] Shin S, Jang J. The effect of amine/epoxy ratio on the fracture toughness of tetrafunctional epoxy resin. Polym Bull 1997;39:353–9.
[42] Kostopoulos V, Baltopoulos A, Karapapas P, Vavouliotis A, Paipetis A. Impact and after-impact properties of carbon fiber reinforced composites enhanced with multi-wall carbon nanotubes. Compos Sci Technol 2010;70:553–63.
[43] Yokozeki T, Iwahori Y, Ishiwata S, Enomoto K. Mechanical properties of CFRP laminates manufactured from unidirectional prepregs using CSCNT-dispersed epoxy. Compos Part A-Appl S 2007;38:2121–30.